Title

Mechanical regulation of cardiac fibroblast profibrotic phenotypes

Journal

Molecular Biology of the Cell, 28(14)

ISSN

1059-1524

Authors

Herum, Kate M

Choppe, Jonas

Kumar, Aditya

et al.

Publication Date

2017-07-07

DOI

10.1091/mbc.e17-01-0014

Peer reviewed

Mechanical regulation of cardiac fibroblast pro-fibrotic phenotypes

Kate M. Herum,[a,b,*] Jonas Choppe,[a] Aditya Kumar,[a] Adam J. Engler,[a,c] Andrew D. McCulloch[a,d]

[a]Department of Bioengineering, University of California San Diego, La Jolla, CA, USA
[b]Institute for Experimental Medical Research, Oslo University Hospital and University of Oslo, Oslo, Norway
[c]Sanford Consortium for Regenerative Medicine, La Jolla, CA, USA
[d]Department of Medicine, University of California San Diego, La Jolla, CA, USA

[*]Corresponding author:
Kate Moller Herum
Department of Bioengineering
University of California San Diego
9500 Gilman Drive
La Jolla
California, 92093-0819
USA
Phone: +1 (858) 999-1257,
Fax: +1 (858) 332-1706
kherum@ucsd.edu

Running head: Mechanical regulation of CFB phenotype

Abstract

Cardiac fibrosis is a serious condition currently lacking effective treatments. It occurs as a result of cardiac fibroblast activation and differentiation into myofibroblasts, characterized by proliferation, extracellular matrix production and stiffening, and contraction due to the expression of smooth muscle α-actin. The mechanical properties of myocardium change regionally and over time after myocardial infarction. Although mechanical cues are known to activate cardiac fibroblasts, it is unclear which specific mechanical stimuli regulate which specific phenotypic trait; thus we investigated these relationships using three *in-vitro* models of cardiac fibroblast mechanical activation and found that: 1) Paracrine signaling from stretched cardiomyocytes induces cardiac fibroblast proliferation under mechanical conditions similar to those of the infarct border region; 2) Direct stretch of cardiac fibroblasts mimicking the mechanical environment of the infarct region induces a synthetic phenotype with elevated extracellular matrix production; 3) Progressive matrix stiffening, modeling the mechanical effects of infarct scar maturation, causes smooth muscle α-actin fiber formation, upregulation of collagen I and downregulation of collagen III. These findings suggest that myocyte stretch, fibroblast stretch and matrix stiffening following myocardial infarction may separately regulate different pro-fibrotic traits of activated cardiac fibroblasts.

Introduction

Cardiac fibroblasts (CFB) are responsible for maintaining extracellular matrix (ECM) composition and organization in the heart wall. They are central mediators of the fibrosis that develops in many forms of cardiac disease, notably myocardial infarction (MI). In response to injury, the CFB becomes activated and acquires a pro-fibrotic phenotype commonly referred to as a myofibroblast (Hinz, 2007), characterized by proliferative activity, excessive ECM production and contractile function due to expression of smooth muscle α-actin (SMA). However, it is becoming increasingly clear that activated CFB display multiple overlapping phenotypes depending on their spatial location and the stage of fibrosis (Tomasek *et al.*, 2002; Hinz, 2007; van Putten *et al.*, 2016). It has been established that the altered mechanical properties of the myocardium associated with cardiac diseases activate CFB (van Putten *et al.*, 2016). However, similar to the heterogeneity of CFB phenotypes, the mechanical alterations occurring in and adjacent to the infarct are regionally variable and change during the acute and chronic phases of infarction and post-infarct remodeling. Therefore, teasing out which mechanical cues regulate specific phenotypic traits may identify novel targets that could prevent the adverse progression of cardiac fibrosis.

CFB mechanosensitivity is demonstrated by their rapid transformation to a pro-fibrotic myofibroblast phenotype when they are grown on plastic tissue culture dishes or polydimethylsiloxane (PDMS) membranes used to impose stretch; these materials have stiffnesses five and three orders of magnitude, respectively, greater than that of cardiac muscle (Berry *et al.*, 2006; Engler *et al.*, 2008). This may explain conflicting reports of both increased and decreased myofibroblast differentiation in response to mechanical stress (Wang *et al.*, 2003; Papakrivopoulou *et al.*, 2004; Husse *et al.*, 2007; Waxman *et al.*, 2012; Guo *et al.*, 2013). Thus, development of cell culture models that better imitate the *in-vivo* mechanical environment and the changes post-infarction are needed (Spinale *et al.*, 2016). The use of hydrogels to manipulate culture substrate stiffness has helped *in-vitro* research on fibroblasts function (Yeung *et al.*, 2005; Goffin *et al.*, 2006; Li *et al.*, 2007; Kloxin *et al.*, 2010; Olsen *et al.*, 2011; Liu *et al.*, 2015), but few studies have investigated the interplay of mechanical stimuli, especially in the context of CFB phenotype plasticity. Thus, all of the experiments here were performed on soft gels with physiological stiffness in an attempt to discriminate the differential effects of substrate stiffness and other applied mechanical stimuli, e.g. biaxial stretch.

To formulate hypotheses for which mechanical forces drive specific CFB responses, it is important to understand the course of events triggered by MI, which roughly equate to acute scar formation and chronic scar remodeling. In the healthy heart, quiescent CFB are probably at least partially protected against large changes in mechanical stress by their physical integration in the structurally stable ECM network. During acute MI, cardiomyocytes (CM) in the ischemic myocardium rapidly cease generating active tension, while contraction of the surrounding functional myocardium gives rise to a functional border zone of perfused and viable tissue that is nonetheless dyskinetic or hypokinetic (Mazhari *et al.*, 2000). The border zone is also associated with CFB proliferation and fibrosis (Virag and Murry, 2003), although the exact mechanism by which fibrosis occurs is unclear; CFB may also be less protected from increased mechanical stress owing to rapid degradation and acute loss of native ECM stiffness. This scenario likely creates excessive stretch during systole, causing CFBs to acquire a synthetic phenotype producing matricellular proteins, structural ECM proteins, and inducing collagen cross-linking

that increases myocardial stiffness (Lopez *et al.*, 2012). In later stages of scar remodeling, CFB differentiation into contractile myofibroblasts and ECM maturation cause scar shrinkage. In the normal adaptive response to scar healing, myofibroblasts undergo apoptosis as ECM tension of the scar is restored and takes over the mechanical load. In conditions where mechanical load continues to be elevated such as in the left ventricles of patients with chronic hypertension, persistent myofibroblast activity and progression of myocardial fibrosis is observed (Creemers and Pinto, 2011). The objective of this study was to investigate the distinct effects and relative contributions of different mechanical stimuli on CFB pro-fibrotic phenotypes. For that, we developed three *in-vitro* models that mimic the mechanical cues of MI. Based on known regional and temporal CFB responses, we hypothesized that: 1) Paracrine signaling from stretched CM induces CFB proliferation; 2) Direct stretch of CFB induces ECM production; and 3) Matrix stiffening promotes a contractile myofibroblast phenotype.

Results

Matrix stiffness affects cardiac fibroblast phenotype and function

To determine the matrix stiffness required for maintaining a quiescent phenotype *in-vitro*, CFB were grown on hyaluronic acid (HA) gels with stiffnesses corresponding to the range of intact myocardial tissue. CFB grown on HA gels with a Young's elastic modulus of 3kPa had low or no expression of the myofibroblast marker SMA (Figure 1A). A substrate stiffness of 8kPa, comparable to that of healthy myocardium (Berry *et al.*, 2006; Engler *et al.*, 2008), was sufficient for formation of SMA fibers. CFB displayed prominent SMA fibers on 50kPa HA gels corresponding to the myofibroblast phenotype observed in fibrotic myocardium which has a stiffness of 20-100kPa (Berry *et al.*, 2006; Engler *et al.*, 2008). Focal adhesion size and location, as determined from vinculin staining, were altered according to substrate stiffness, transitioning from small peripheral adhesions on 3kPa substrates to large "super mature" focal adhesion structures that were evenly distributed throughout the cell membrane on 50kPa substrates (Figure 1B). Although adhesion changes were more continuous, CFB area was markedly higher at and above 8kPa than for 3kPa HA gels (Figure 1C). Proliferation rate was similar for all stiffnesses (Figure 1D). We observed local the lowest mRNA expression for extracellular matrix remodeling genes in CFB on 8kPa HA gels (Figure 1E), with the notable exception of thrombospondin 1 (THBS1). These data indicated that culturing CFB on HA gels with stiffness of 3 and 8kPa maintained the quiescent phenotype, thus these stiffnesses were used in the subsequent *in-vitro* assays. Since we also used polyacrylamide (PA) gels in this study, phenotyping experiments for SMA fiber incorporation and proliferation were repeated for CFB on PA gels and showed no significant difference to HA gels (Supplementary Figure 1).

Paracrine signaling from stretched cardiomyocytes induces proliferation of cardiac fibroblasts

CM and CFB were first cultured on separate substrates with common culture media (Figure 2A) to assess paracrine communication during CM stretch. CM were subjected to non-equibiaxial biaxial (14% longitudinal, 3.6% transverse) static stretch using a custom device mimicking strains in the border region post-MI *in-vivo* (Camelliti *et al.*, 2006). Proliferation of the non-stretched CFB markedly increased in the presence of CM and was further enhanced by their stretch (Figure 2B). Whereas CM stretch was necessary to induce proliferation of grown on 8kPa substrates, CFB on 3kPa substrates also responded to paracrine signaling from non-stretched CM

(Supplementary Figure 2A), indicating enhanced sensitivity of CFBs to paracrine signals. CFB proliferation rates were similar on 3 and 8kPa substrates when cultured with stretched CM, suggesting that responses to stretch-induced paracrine signaling are independent of substrate stiffness. The effect on CFB proliferation was not significant when CFB were treated with conditioned media from stretched CM, i.e. without the co-culture device, possibly indicating that paracrine mediators have short half-lives (Figure 2C). A co-culture media screen indicated significant presence of a subset of cytokines, (Supplementary Figure 2B) and among these, mRNA of CSF-1 and platelet-derived growth factor B (PDGF-B), a growth factor known to induce proliferation of mesenchymal cells (Antoniades *et al.*, 1979) were upregulated in stretched CM (Figure 2D). Although fibroblast growth factor 2 (FGF2) mRNA increased with 24h stretch, it was reduced at the earlier time point, suggesting that this factor is not the initiator of CFB proliferation. Stimulation of CFB on 8kPa-substrates with recombinant CSF-1 or PDGF-B induced CFB proliferation, and this response was enhanced by co-stimulation with both factors (Figure 2E). Finally, treatment with PDGF-B (AG-1295) and CSF-1 (GW-2580) receptor antagonists prevented the increase in CFB proliferation observed in co-cultures with stretched CM, suggesting PDGF-B and CSF-1 to be central to the paracrine signaling induced by stretch. Treatment with antagonists also reduced the proliferative response of CFB on 8kPa PA gels (Figure 2F), indicating a basic level of PDGF-B and CSF-1 receptor activity. This effect was abolished when CFB were co-cultured with non-stretched CM. Despite effects on proliferation, paracrine signaling from stretched CM had no effect on SMA fiber formation or FN expression (Supplementary Figure 2C-E). There was a slight reduction in cell area (Figure 2G), possibly as a result of the increased proliferation or morphological changes such as enhanced cell protrusions (Figure 2H), which may reflect cell responses to chemotactic agents in the media. Overall, these data are suggestive of a direct effect of CM stretch on CFB proliferation via paracrine CSF-1 and PDGF-B signaling.

Stretching cardiac fibroblasts on soft substrates induces SMA and ECM expression

To stretch CFB grown on substrates of physiological relevant stiffness and thus maintained as inactivated quiescent fibroblasts, 3 and 8kPa PA gels were attached to PDMS membranes (Figure 3A) using a previously published protocol (Simmons *et al.*, 2013). Static 3% or 6% equibiaxial stretch (corresponding to a 10% and 20% cell area change, respectively (Lee *et al.*, 1999) was applied using a custom circular stretch device (Camelliti *et al.*, 2006). Although static stretch of the PA gels was sustained for 24h, cells returned to their original size well within the 24h of applied stretch (Supplementary Figure 3). Nevertheless this static stretch induced massive upregulation of mRNA for collagen 1a1, collagen 1a2, collagen 3a1 and fibronectin (Figure 3B) and protein for fibronectin (Figure 3C). The effect was more prominent in CFB on 8kPa PA gels and independent of stretch amplitude. Other ECM remodeling genes were also altered by 3% stretch (Figure 3D) with tenascin C (TNC) being the only oppositely expressed gene between 3kPa and 8kPa substrates. Stretch also induced opposing proliferation responses depending on substrate stiffness (Figure 3E).

SMA mRNA levels were markedly substrate dependent with 300- and 8-fold increases for the 3 and 8 kPa PA gels (Figure 3F). This was also reflected in immunostaining for SMA where SMA intensity was clearly increased in 3kPa CFB cultures after stretch, albeit not incorporated into fibers (Figure 3G). Although development of SMA fibers was not induced by stretch, cell morphology of 8kPa CFB cultures was altered by stretch displaying more elongated cells, suggesting that cells remodel and readjust cell size during the 24h static stretch.

Since vinculin staining (Figure 1) showed differences in focal adhesion size for CFB on 3 and 8kPa substrates, we measured activation (by phosphorylation) of focal adhesion kinase (FAK). FAK was phosphorylated by 24h static stretch only in CFB on 8kPa suggesting active mechanotransduction by integrins (Figure 3H).

TGFβ is the most well-known driver of myofibroblast differentiation (Biernacka *et al.*, 2011), and mRNA levels were increased by stretch only in CFB on 3kPa PA gels (Supplementary Figure 4A). However, this was not accompanied by TGFβ activity 24h after static stretch (Supplementary Figure 4B) and TGFβ activity was reduced by stretch for CFB on 8kPa PA gels. TGFβ is known to regulate expression of the myofibroblast marker gene fibronectin extradomain A (EDA) which also was increased in CFB on 3kPa but reduced in CFB on 8kPa PA gels following stretch (Supplementary Figure 4C), supporting that EDA may be down-stream of TGFβ signaling and not independently regulated by stretch. Accompanying higher fibronectin protein staining (Supplementary Figure 4D), mRNA levels of αv, a fibronectin receptor and TGFβ-activing integrin, were higher in CFB on 3kPa compared to 8kPa substrates (Supplementary Figure 4E), suggesting that these CFB are more capable of activating TGFβ. Collectively, these data suggest an interplay between substrate stiffness and stretch to induce a synthetic phenotype, but in a limited set of niche conditions.

Matrix stiffening from physiological to pathological stiffness induces upregulation of collagen I, downregulation of collagen III and smooth muscle α-actin fiber formation

Since stretch effects depend on local stiffness, it is important to note that stiffness itself depends on ECM production and crosslinking, and this can increase during scar formation post-infarct. To determine how dynamic changes in stiffness could affect CFBs, cells where grown on soft (3 or 8kPa) HA gels for 5 days before stiffening substrates to 30kPa (Figure 4A); Although this treatment is UV based, we did not observe p53 immunostaining and viability changes suggestive of cell damage (Supplementary Figure 5). To detect changes in SMA expression and fiber formation, HA gels were stiffened from 3kPa (where CFB have no SMA fibers) to 30kPa. Stiffening caused massive cell spreading, increased SMA intensity and SMA fiber formation (Figure 4B). Similar to CFB on 10kPa HA gels (see Figure 1A), SMA fibers were present at 8kPa (Supplementary Figure 6A) and stiffening from 8 to 30kPa did not induce additional presence of SMA fibers or cell spreading. These data suggest that the threshold for SMA fiber formation in 2D cultures is somewhere in the range of >3kPa to <8kPa. TGFβ and EDA mRNA were unchanged after stiffening from 3 to 30kPa and 8 to 30kPa (Supplementary Figure 6B) indicating that the effect on SMA was a direct effect of stiffening and not downstream of TGFβ signaling. Stiffening from 8 to 30kPa increased collagen I but reduced collagen III mRNA as measured 24h after stiffening (Figure 4C), suggesting differential transcriptional regulation of these two genes. Although fibronectin mRNA expression was not was upregulated in CFB 24h after stiffening, immunofluorescent staining intensity of fibronectin protein was increased 48h after stiffening from 8 to 30kPa (Figure 4D). No change was observed for LOX mRNA (Figure 4C) or activity (Supplementary Figure 6C), nor was there any change in other ECM proteins after stiffening from 8 to 30kPa (Supplementary Figure 6D). Interestingly, osteopontin mRNA was reduced following substrate stiffening from 8 to 30kPa (Figure 4C) even though this gene has previously been found to upregulated in response to mechanical stress (Herum *et al.*, 2015). Proliferation was unchanged by stiffening from 8 to 30kPa (Supplementary Figure 6E). Taken

together, these data specifically imply that SMA expression and its assembly are affected by temporal changes in passive niche properties, e.g. stiffness.

Discussion

In these studies we found that: 1) Paracrine signaling from stretched CM induces proliferation of CFB, consistent with the high proliferative activity of fibroblasts in the functional border region after acute MI (Figure 5, point 1); 2) ECM production by CFB in response to stretch is dependent on matrix stiffness. This suggests a mechanism for differential regulation of ECM across the infarct and peri-infarct regions during the acute phase when ECM stiffness is decreased due to rapid degradation of ECM (Figure 5, point 2a), and the subsequent remodeling phase when ECM stiffness increases with the accumulation of newly synthesized ECM (Figure 5, point 2b); 3) Matrix stiffening induces massive cell spreading and SMA fiber formation as hypothesized. We also report the novel finding that substrate stiffening promotes collagen I but inhibits collagen III expression (Figure 5, point 3). This response imitates the late stages of infarct healing when ECM stiffening dominates the mechanical environment of the infarct scar. Figure 5 summarizes the results in the context of the mechanics of myocardium following MI.

Matrix stiffness regulates fiber formation while stretch regulates expression of smooth muscle α-actin

For the first time, we here show the effect of matrix stiffening on CFB phenotype, causing massive cell spreading and incorporation of SMA into stress fibers. This is in agreement with reports from other fibroblast-like cells, including hepatic stellate cells (Guvendiren *et al.*, 2014; Caliari *et al.*, 2016), mesenchymal stem cells (Guvendiren and Burdick, 2012) and the NiH3T3 fibroblast cell line (Ondeck and Engler, 2016). Although equibiaxial stretch also caused a dramatic increase in SMA mRNA, it did not promote SMA stress fiber formation, suggesting that substrate stiffness is the dominant determining mechanical factor for the assembly of SMA into fibers and subsequent contraction of the infarct scar. From a mechanical standpoint this is consistent with the cell tensegrity theory (Ingber, 2008). Interestingly, Cui and colleagues showed that cyclic stretch of CFB on soft gels did induce F-actin stress fibers even in the absence of matrix stiffening (Cui *et al.*, 2015). Whether this also applied to SMA fiber formation was not studied. The massive upregulation of SMA mRNA in stretched CFB on 3kPa PA gels might partly be due to increased TGFβ signaling, since TGFβ and its target gene EDA also exhibited increased expression following stretch. This was not the case for CFB on 8kPa substrates suggesting a mechanotransduction pathway independent of TGFβ to account for this change, e.g. mechanotransduction *via* the transmembrane proteoglycan syndecan-4 has been shown to have such an effect (Herum *et al.*, 2013).

Mechanical cues regulate collagen differentially

Essential for development of fibrosis is enhanced production of structural ECM proteins, with collagen amount and composition being of particular importance due to its central role in myocardial stiffening. Stretch (3%, 8kPa substrates) caused massive upregulation of collagen III

and fibronectin, thus confirming our previous results from CFB stretched on PDMS substrates (with an elastic modulus in the MPa range) (Lee *et al.*, 1999). However, responses by CFB on soft substrates were 5- and 2.5-fold higher for collagen III and fibronectin, respectively, suggesting a more mechanosensitive CFB phenotype in this setting. Also, increasing stretch to 6% did not reduce fibronectin mRNA as previously reported for standard PDMS membranes (Lee *et al.*, 1999), again supporting different responses to stretch depending on substrate stiffness. Both stretch and substrate stiffening promoted collagen I expression, although the response was ten times higher for stretch in the case of col1a1. Interestingly and in contrast to stretch, collagen III was downregulated in response to stiffening. Mass spectrometry has provided insight about the ECM composition of infarct regions (Sullivan *et al.*, 2014), indeed showing elevated collagen I and reduced collagen III levels in the mature scar compared to earlier stages of remodeling. Along these lines, collagen I and III ratio has been suggested to influence myocardial stiffness, with high collagen I:III ratio being associated with a less compliant ventricle (Mukherjee and Sen, 1990). Also other subtypes of collagens including non-structural collagens have been associated with cardiovascular disease (Rasi *et al.*, 2010; Luther *et al.*, 2012; Skrbic *et al.*, 2015). Determining the mechanoregulation and role of these less studied collagens may provide valuable information for evaluating their importance in different stages of cardiac fibrosis development.

Collagen maturation is promoted by stretch

Collagen cross-linking is emerging as an essential player in myocardial stiffening and diastolic dysfunction (Kasner *et al.*, 2011; Lopez *et al.*, 2012). mRNA for the collagen cross-linking enzyme LOX and its activator BMP1 were increased by stretch, but no change in LOX mRNA and activity were observed after matrix stiffening, suggesting the absence of a feed-forward loop involving further stiffening by enzymatic collagen cross-linking. In agreement, OPN and POSTN, which are known to induce LOX expression (Lopez *et al.*, 2013; Herum *et al.*, 2015) and increase collagen cross-linking (Maruhashi *et al.*, 2010) were not upregulated by substrate stiffening. Thus stretch seems to be the mechanical trigger for enzymatic collagen cross-linking. Indeed LOX has been shown to become rapidly upregulated prior to myocardial stiffening in an experimental mouse model of left ventricular pressure overload (Herum *et al.*, 2015). Cross-linked collagen is less susceptible for degradation by the MMP enzymes. This, together with the increase in MMP endogenous inhibitors TIMP1 and 2 by CFB on 3kPa PA gels, supports that stretch promotes collagen maturation and ECM stabilization.

The effect of stretch on matricellular gene expression is dependent on matrix stiffness

Matricellular proteins such as OPN, POSTN, SPARC and THBS1 play important roles in post-MI remodeling, and were upregulated by stretch when cells were cultured on 3kPa but not 8kPa PA gels. A stiffness of 3kPa likely reflects the ECM stiffness in the early phase after an infarct where a sudden increase in MMP activity (Takahashi *et al.*, 1990) leads to degradation of collagen and thus decreases myocardial stiffness. Indeed, results from experimental animal models of MI and left ventricular pressure overload generally show a rapid increase of OPN, POSTN and SPARC at early stages and a somewhat decline at later stages of ECM remodeling (Schellings *et al.*, 2009; Sullivan *et al.*, 2014; Herum *et al.*, 2015). As new ECM accumulates and remodeling of the infarct progresses, myocardial stiffness will gradually increase. Reflecting the mechanical environment of this stage of remodeling, osteopontin mRNA was reduced with stretch of CFB on 8kPa PA gels. Interestingly, cardiac MMPs have recently been found to cleave OPN resulting in OPN fragments with distinct biological functions that are associated with

fibrosis (Lindsey *et al.*, 2015). Thus, a stiffness resembling the healthy myocardium or later stages of post-MI remodeling may exert a negative feedback effect on fibrosis development.

Possible mechanisms for stiffness-specific stretch responses

Although mechanical activation of FAK has been studied extensively (Parsons, 2003; Wong *et al.*, 2012), we here show that stretch-induced activation is stiffness-dependent and could therefore be involved in the stiffness-specific response of CFB to stretch. Indeed, stiffness has been shown to be a regulator of FAK activity (Carraher and Schwarzbauer, 2013) and required for nuclear translocation of the transcriptional cofactor four-and-a-half LIM domains 2 (FHL2) which controls cell proliferation by modulating p21 gene expression (Nakazawa *et al.*, 2016). This is in agreement with the stiffness-dependent inhibition of proliferation observed along with FAK activation. FAK is activated by integrins in response to mechanical stress, and signals downstream to activate mitogen-activated protein kinases (MAPK) signaling (Hynes, 2002), known to induce myofibroblast differentiation and ECM production (Davis and Molkentin, 2014; Lighthouse and Small, 2016; Molkentin *et al.*, 2017), and inhibition of FAK was recently successfully used to prevent fibrosis after myocardial infarction (Zhang et al., 2017). Thus, inhibition of FAK may hold therapeutic potential for treatment of cardiac fibrosis and it is therefore important to understand which mechanical cues regulate its activity in cardiac fibroblasts. Although we did not see increased TGFβ activity in CFB on 3kPa PA gels 24h after static stretch, there were other indications that TGFβ signaling was enriched only for CFB on 3kPa substrates. Collectively, our data indicate that the stiffness of the ECM directly surrounding the CFB seems to influence which pro-fibrotic signaling mechanisms are activated by stretch.

Matrix stiffness dictates the effect of stretch on TNC expression

The matricellular protein TNC distinguished itself from the other matricellular proteins in that it exhibited regulation in opposite directions according to matrix stiffness, being downregulated on 3 and upregulated on 8kPa PA gels in response to stretch. Interestingly, TNC expression post-MI is seen in regions expected to have mechanical properties resembling the stiffer 8kPa PA gels including the viable border zone during acute MI and the central infarct zone during the chronic stages of remodeling where it is co-expressed and co-localized with fibronectin (Willems *et al.*, 1996). The different domains of TNC have distinct functions that manifest themselves according to the environment. TNC can disrupt CM adhesions at the CM costameres thereby facilitating tissue reorganization in the border region after MI (Imanaka-Yoshida *et al.*, 2001), while promoting myofibroblast differentiation in the infarct region during the remodeling phase (Duerr *et al.*, 2011). The differential TNC gene expression demonstrated here suggests a critical importance of matrix stiffness in determining the specific mechanosignaling pathways are engaged in response to stretch.

Paracrine signaling from stretched cardiomyocytes induces cardiac fibroblast proliferation via PDGF and CSF-1

The main effect of paracrine signaling from stretched CM was enhanced proliferation of CFB and this response was independent of substrate stiffness. This resembles the intense proliferative activity of fibroblasts present in the border zone and infiltrating the infarct region (Virag and Murry, 2003). Results from immunohistochemical studies and *in-situ* hybridization experiments suggest that stretched CM in the infarct border zone produce a variety of cytokines

(Gwechenberger *et al.*, 1999) and chemokines (Tarzami *et al.*, 2002). However, the identity and relative contribution of CM-derived inflammatory mediators for the pro-fibrotic response of CFB is poorly understood. We here identify PDGF-B and CSF-1 as factors upregulated in CM by stretch and capable of inducing the observed response on CFB proliferation. Whereas PDGF has been shown to be rapidly upregulated in the border zone (Zhao *et al.*, 2011), and promote proliferation of rat atrial fibroblasts (Jiang *et al.*, 2016), studies on the effect of CSF-1 on CFB are limited although it does regulate the survival, proliferation, and differentiation of mononuclear phagocytes (Chitu and Stanley, 2006) and can be expressed by cardiac cells (Hohensinner *et al.*, 2007). Antagonists for PDGF-B and CSF-1 receptors could prevent the increase in proliferation of CFB induced by paracrine signaling from stretched CM, supporting a role for PDGF-B and CSF-1 in CM-induced proliferation.

Limitations of the *in vitro* CFB models

The static stretch is a model of a chronic hemodynamic overload such as an increase in ventricular volume, rather than the effects of phasic cardiac strains. Although cyclic stretching does more closely reflect the contraction cycle of the heart, *in-vitro* models do not recapitulate the frequencies of cyclic strain of the mouse heart (≈10Hz). Previously published work show that low frequency (0.1Hz) cyclic strain of CFB on soft substrates display greater SMA fiber formation (Cui *et al.*, 2015). This would either suggest the sustainment of a mechanical memory as was recently demonstrated for microRNA-21 in mesenchymal stem cells (Li *et al.*, 2017), or that the continuous cyclic stretch prevents cells from remodeling back to their original size, as we observed for 24h static stretch. The fact that we saw dramatic responses to static stretch that mimic the cardiac fibroblast responses observed after myocardial infarction *in-vivo*, supports that pathological remodeling is mainly driven by an increase in baseline stretch.

Conclusion and future perspectives

Antifibrotic therapies have failed owing to the pleiotropy of targets and difficulties of regional and temporal targeting of the post-infarcted myocardium. For instance, while blocking well-known fibrotic pathways inhibits excessive fibrosis and diastolic dysfunction, cardiac rupture becomes more prevalent (Daskalopoulos *et al.*, 2012; Hermans *et al.*, 2016). Hence, it may be necessary to promote myofibroblast transformation in some regions and certain times (e.g. to stabilize ECM in the infarct zone at early stages of post-MI remodeling), while inhibiting their actions in other (e.g. preventing fibrosis in remote and border regions during the chronic stages of post-MI remodeling). Although many of our observations have been made in other cell types, this study provides new information about pro-fibrotic responses of cardiac fibroblasts to specific and distinct mechanical cues, which occur *in-vivo* in the complex mechanical milieu of post-myocardial infarction remodeling. Further, our results suggest that the engaged mechanotransduction pathways are specific to particular mechanical cues. With these novel experimental tools and established CFB phenotypes in place, differential targeting of mechanosignaling pathways present at different stages and regions of fibrosis development, is an obtainable goal. These targets include components of the extracellular matrix itself, such as the family of proteoglycans of which accumulating data support a central role in cardiac mechanosignaling and differential expression patterns at different stages of fibrosis development (Melchior-Becker *et al.*, 2011; Engebretsen *et al.*, 2013; Lunde *et al.*, 2016; Melleby *et al.*, 2016). Another approach that holds great promise is the combination of high sensitivity analyses of entire CFB transcriptomes and advanced systems biology computational models (McCulloch, 2016; Zeigler *et al.*, 2016) to draw connections between changes at the transcriptional level to

upstream signaling pathways as well as downstream phenotypic changes. In this way, established signaling pathways may prove to play previously unknown roles in mechanotransduction, and novel pro-fibrotic mechanosensitive signaling pathways may be identified.

Materials and methods

Isolation of adult cardiac fibroblasts

CFB were isolated from adult CD1 male and female mice (Charles River Labs, San Diego, CA, USA) and all animal procedures followed the Guide for the Care and Use of Laboratory Animals (Eighth Edition) and were approved by UCSD Animal Subjects Committee (Protocol#S01013M). Mice were euthanized by cervical dislocation after initial anesthesia with "open drop" isoflurane. Hearts were excised, rinsed in Hank's Balance Salt Solution (HBSS, Cat#14170-120, Gibco Life Technologies, Grand Island NY, USA) and the left ventricle cut into 8 pieces. These were subjected to pre-digestion in 0.6mg/ml trypsin (Cat#22715, USB, Cleveland OH, USA) overnight at 4°C. Hearts were further digested with 1mg/ml (330U/ml) collagenase type 2 (Cat#LS004176, Worthington Biochem, Lakewood, NJ, USA) for 10min at 37°C and mechanically dissolved by repeated pipetting. Cell solution was passed through a 100µm cell strainer whereafter the collagenase was neutralized by adding Fibroblast media consisting of Dulbecco's Modified Eagle's Medium (DMEM; Cat# 11965-092, Gibco Life Technologies) supplemented with 10% fetal bovine serum (FBS; Cat#16000-044, Gibco Life Technologies) and 1% antibacterial/antimicrobial (Sigma, St.Louis, MO, USA). The cell solution was centrifuged at 200g for 4min, whereafter the supernatant was aspirated and the pellet resuspended in fibroblast media. The solution was then incubated in a T75 tissue culture flasks for 30min at 37ºC and 5% CO_2 allowing fibroblasts to attach to the flask so that the supernatant containing CM and ECM debris could be removed. CFB were immediately trypsinized in 0.05% Trypsin-EDTA (Cat#25300-054, Gibco Life Technologies), counted and seeded onto PA or HA gels for further experiments.

Isolation of neonatal cardiomyocytes

Neonatal CD1 mouse pups (Protocol#S01013M, Charles River Labs) were euthanized by decapitation and hearts removed and rinsed in HBSS. Pre-digestion was performed with 0.46mg/ml trypsin overnight and digestion with 0.7mg/ml collagenase type 2 for 7 min at 37°C. Further digestion was done by repeated pipetting whereafter the cell solution was passed through a 100µm cell strainer. Collagenase was neutralized by adding Dark media consisting of 3:4 DMEM, 1:4 M-199 (Cat#11150-059, Gibco Life Technologies) and supplemented with 1% HEPES (1M), 10% horse serum (Cat#DH-05, Omega Scientific, Tarzana, CA, USA), 5% FBS and 1% penicillin/streptomycin (Cat#30-00261, Corning, Manassas, VA, USA). The cell solution was centrifuged at 200g for 4min. After resuspending the pellet in dark medium, pre-plating was performed by letting non-CM cells attach to T75 flasks for 1.5h at 37°C and 5% CO_2. The supernatant containing CM was collected, centrifuged for 4min at 200g and resuspended in 2ml Dark media. Cell number was determined using a Bürcher cell counter chamber by counting live cells after the addition of Trypan Blue (Cat#K940, VWR Amresco,

Solon, OH, USA). 700,000 CM were added to each cell stretcher membrane and incubated at 37°C and 5% CO_2 for 3 days before stretch experiments were performed. For some control experiments 10μM AraC (Cytosine-B-D-arabino-furanoside hydrochloride; Cat#C6645, Sigma) was added on day 2 after isolation to prevent survival of "contaminating" CFB (Ehler *et al.*, 2013).

Preparation of polyacrylamide gels

PA gels were fabricated with Elastic Moduli *E* of 3.13 (3kPa) and 8.7kPa (8kPa) by adjusting the relative acrylamide and bis-acrylamide concentrations (Tse and Engler, 2010). 0.5% acrylic acid was added to enable subsequent collagen attachment. The photoinitiated cross-linker Irgacure 2959 (Sigma) was dissolved in 100% ethanol to obtain a 10% solution which was then diluted to 0.05% in the PA solution. PA solution was then sandwiched between a 12mm diameter coverslip that was UV-ozone activated and methacrylated to permit hydrogel binding, and a glass slide that was treated with dichlorodimethylsilane (DCDMS, Cat#430881000 Acros Organics, Geel, Belgium) to avoid adherence to the gel. To initiate gel polymerization, the hydrogel was subjected to UV light with a wavelength of 350nm for 5min using a transilluminator (4 mW/cm2; UVP, Upland, CA, USA)

PDMS membrane

Two-part polydimethylsiloxane (PDMS, Cat#30097358-1004, Sylgard 186, Dow Corning, Midland, MI, USA) was mixed at a 10:1 ratio of base to curing agent according to the manufacturer's instructions. The mixture was then loaded into 10mL syringes with Luer-Lok stopcocks, and large air pockets were removed in an IEC Centra CL2 centrifuge at 2500rpm for 3min. Seven mL of elastomer mix was then extruded onto either an unpatterned or a patterned (microgrooves of 10μm width, 5μm depth and spaced 10μm apart) silicon wafer in a spin coater. The spin coater was run at 650rpm for 30s for each wafer. All wafers were then placed in a vacuum chamber to degas in short cycles for 20-40min, or until all visible bubbles were gone. The wafers were then oven cured for 30min at 70ºC, and cooled at room temperature overnight. The membranes could then be peeled off the wafer and stored in a clean environment for up to 1 year (Camelliti *et al.*, 2006).

Treatment of PDMS membranes with benzophenone in to allow polyacrylamide adherence

In order to allow PA gel adherence to the PDMS surface, a previously described protocol (Simmons *et al.*, 2013) was utilized. The silicone elastomer PDMS membranes were immersed in a solution of 10% benzophenone (Cat#A10739, Alfa Aesar) dissolved in a water/acetone mixture (35:65 w/w) for 1min. The membranes were then immediately rinsed with methanol and dried with a stream of nitrogen. Following benzophenone treatment, PA gel solution was prepared as described above, pipetted onto the surface of the membrane, covered with a DCDMS-treated 25mm coverslip and exposed to UV light (350nm) for 25min. Coverslips were removed and gels that successfully adhered to PDMS membranes were equilibrated in PBS overnight.

Assembly and stretch of circular and elliptical stretch device

Prior to coating with protein, PDMS membranes were assembled in circular (for CFB on PA gels on unpatterned PDMS stretch membranes) or elliptical (for CM on patterned PDMS stretch membranes) in-house built stretch devices (Camelliti *et al.*, 2006). A perimeter of silicone grease was placed around the area intended for cell attachment and coated with either collagen I for

CFB cultures or laminin (10µg/ml, 10min UV exposure, Cat#L2020, Sigma) for CM cultures. After 3 days of cell culture, static stretch was applied for 24 and 48h by turning the screw top of each device to the extent corresponding to the desired amount of stretch. Stretch has previously been confirmed to transfer to cells cultured on PA gels attached to PDMS stretch membranes (Simmons *et al.*, 2013). To determine whether cells return to their original size after stretch, cell area of 8 cardiac fibroblasts on PDMS stretch membranes was measured before stretch, immediately after stretch and 10, 20, 30 and 60 min after applying static stretch. Cell areas for non-stretched and stretched CFB on 3 and 8kPa PA gels were measured 24h after applying the static stretch.

Interface co-culture device for studying paracrine signaling in combination with stretch
To study the effect on paracrine signalling from stretched CM on CFB phenotype, we designed a co-culture device that allowed CFB on PA gels attached to coverslips to be inverted onto CM in the elliptical stretch device while preventing physical contact between cell cultures. The design allowed sufficient gas exchange, close proximity (1mm) between cell cultures to ensure maximum effect of paracrine signals, easy access to media, easy collection of CFB cultures after completion of the experiment and was made of a biocompatible inert material (polylactic acid, PLA). The device was manufactured by 3D-PLA printing. CM were stretched by rotating the screw-top 720°C, corresponding to a 14% longitudinal and 3.6% transverse stretch of the CM. CFB and media were collected after 24 or 48h co-culture.

Production and stiffening of hyaluronic acid hydrogels
HA was methacrylated and HA hydrogels synthesized according to the protocols described by the Burdick (Guvendiren *et al.*, 2014) and Engler (Ondeck and Engler, 2016) groups. Sodium hyaluronate (50 kDa, Lifecore Biomedical, Chaska, MN, USA) was dissolved in de-ionized water overnight whereafter 20M methacrylate anhydride was added for an additional 12h, dialyzed against de-ionized water at 4°C for 3 days and lyophilized for an additional 3 days. Hydrogels were synthesized by dissolving methacrylated hyaluronic acid at 1% in PBS containing 0.2M triethanolamine (Sigma). HA hydrogel solution containing 0.02% Irgacure 2959 was sandwiched between a 12mm diameter coverslip that was UV-ozone activated and methacrylated, and a DCDMS-treated glass slide. To induce gel polymerization, the hydrogel was subjected to UV light with a wavelength of 350nm for 0.5-2min using a transilluminator. HA hydrogels were stiffened by incubating 30min with 0.05% v/v Irgacure 2959 per 1ml cell media consisting of DMEM without phenol red (Cat#SH30284.01, GE Life Sciences, Logon, UT, USA) supplemented with 10% fetal bovine serum prior to 2min exposure to UV light (350nm). Cell cultures were immediately washed three times with cell media. Atomic Force microscopy (MFP-3D-Bio atomic force microscope, Asylum Research; Santa Barbara, CA) was used to determine hydrogel elastic modulus as previously described (Ondeck and Engler, 2016). To ensure that UV exposure was not detrimental to cells, live-dead stain (Cat#R37609, Molecular Probes, Eugene, OR, USA) and immunostaining for p53 was performed.

Collagen attachment to PA and HA gels
Collagen I from rat tail was attached by incubating PA gels with 20mM 1-ethyl-3-(3-dimethylaminopropyl) carbodiimide (ProteoChem, Hurricane, UT, USA), 50mM N-hydroxysuccinimide (Alfa Aesar, Heysham, UK), and 100µg/ml type I rat tail collagen (Cat#354249, BD Biosciences, Bedford, MA, USA) dissolved in phosphate-buffered saline (PBS) overnight at 37ºC. To fluorescently label collagen on the surface of the hydrogel to

compare amount of rat tail type I collagen binding to HA and PA hydrogel, a polyclonal rabbit type 1 collagen antibody (1:200, Novus Biological NBP1-30054) and 568 conjugated goat anti-mouse secondary antibody (1:1000, Thermo A-10042) were used. Confocal cross-sections of hydrogels were taken and intensities were obtained using ImageJ (NIH) and plotted using Matlab. Collagen staining intensity was normalized to background and the maximum intensity was used to quantify relative collagen amount. Values were normalized to amount found on HA gels.

Proliferation assay

Proliferation was measured with the Click-iT® EdU imaging kit (Cat#C10337, Life Technologies, Grand Island, NY), according to the manufacturer's instructions and imaged and analysed with the EVOS FL Auto fluorescence microscope (Cat#AMAFD1000, Life Technologies). Ten pictures were taken per gel at 10X magnification and EdU and DAPI positive nuclei were counted and represented as the fraction of proliferating cells per 24h. CFB were stimulated with 10ng/ml recombinant PDGF-B (Cat#558802, BioLegend, San Diego, CA), 10ng/ml CSF-1 (Cat# 14-8983-62, Affymetrix, San Diego, CA) and their respective receptor blockers AG1295 (10µM, Cat#ab142375, Abcam, Cambridge, MA, USA) and GW2580 (5µM, Cat#SML1047, Sigma).

Activity assay

LOX and TGFβ activity was measured in the media of CFB cultures 24h after stiffening using a LOX activity assay (Cat#ab112139, Abcam) and TGFβ activity assay (Cat#437707, BioLegend, San Diego, CA, USA) according to the manufacturer's instructions.

Immunocytochemistry

CFB were fixed in 4% paraformaldehyde, permeabilized in 0.1% Triton X (Sigma), quenched with 25mM glycin (Cat#646500, Fischer Scientific, Fair Lawn, NJ, USA), blocked in 5% goat serum (Cat#G6767, Sigma) in PBS for 20 min, and incubated at 4ºC overnight with primary antibodies toward SMA (1:200, mouse anti-mouse α-SMA, Cat#A5228, Sigma), fibronectin (1:200, rabbit anti-mouse fibronectin Cat#ab2413, Abcam), vinculin (1: 200, mouse anti vinculin Cat#V9131, Sigma) and p53 (1:200, rabbit anti-p53 Cat#sc6243, Santa Cruz Biotechnology, Santa Cruz, CA, USA) in 2% goat serum in PBS. After washing three times 10min with PBS, secondary antibodies were added (1:1000 in 2% goat serum, AlexaFluor488 goat anti-mouse Cat#A11029, AlexaFuor700 goat anti-rabbit Cat#A21038, Molecular Probes). 633-Phalloidin (1: 200 in PBS, 20min at room temperature, Cat#A22284, Molecular Probes) was used to stain F-actin and DAPI used to stain nuclei. Coverslips with cells were mounted on microscope slides using SlowFade® Gold antifade reagent (Cat#S36940, Molecular Probes) and imaged and analysed with the EVOS FL Auto fluorescence microscope. Fibronectin was imaged with 20X magnification and the staining intensity was analysed using Image J (1.50f). Settings were kept constant for the same experiment (from a same date), time point and stiffness. The presence of SMA fibers was evaluated for at least ten micrographs per gel at 20X magnification. For some micrographs EdU proliferation assay and SMA staining were performed simultaneously at the same excitation and emission wavelength. Since EdU was restricted to the nucleus and SMA is located in the cytosol, these were easily distinguished during analysis. Cell area was measured by using brightness and contrast thresholds that clearly displayed the autofluorescence of the cell

cytoplasm and thus enabled automatic quantification of the area of the micrograph covered with cells. This area was then divided by the number of cell nuclei as determined by DAPI staining.

RNA isolation, cDNA synthesis and real-time PCR

RNA isolation was performed using the TRIzol method. First, 1mL of TRIzol (Cat#15596026, Ambion, Carlsbad, CA, USA) was added to each of the gels in order to lyse CFB. The cell lysate was then added to pre-spun Phase Lock Gel-Heavy tubes (Cat#2302830, 5 Prime GmbH, Hamburg, Germany), spun at 1500g for 30s and incubated for 5min at 22ºC. 0.2mL of chloroform was then added to each gel and shaken vigorously for 15s. The lysate/chloroform mixture was then centrifuged at 12,000g for 10min at 4ºC. Following this spin, there was a visible separation between the layers of solution with a clear aqueous layer entirely above the Phase Lock Gel. This aqueous layer, containing RNA, was then removed and placed into a fresh 1.7mL tube. To each of the RNA solutions, 0.5mL of isopropyl alcohol was added and mixed by inversion. Samples were then allowed to incubate at 22ºC for 10min followed by centrifugation for 10min at 12,000g (4ºC). The supernatant was then decanted and 1mL of freshly prepared 75% ethanol was added to each sample. 1µL of glycogen was added to each sample to visualize the pellet. Samples were then centrifuged for 5min at 7,500g (4ºC). Following this centrifugation, the supernatant was decanted from each sample and the RNA pellet was dried. Finally, each RNA pellet was resuspended in 15µL of Molecular Biology Grade water and stored for later quantification and analysis. For CFB on stretchers, RNA isolation was performed with RNeasy minikit (Cat#74104, Qiagen, Hilden, Germany) according to the manufacturer's protocol. RNA quantification was performed with the Qubit RNA BR assay kit (Cat#Q33211, Molecular Probes) and cDNA synthesis using the iScript kit (Cat#04896866001, Roche, Indianapolis, IN, USA) according to the manufacturer's protocol. Quantitative real-time PCR was performed using StepOnePlus Real-time PCR machine (Applied Biosystems, Foster City, CA, USA) and KAPA SYBR Fast Universal qPCR kit (Cat#07959397001, Kapa Biosystems, Cape Town, South Africa) and primers targeting the genes of interest (Integrated DNA Technologies, Indianapolis, IN, USA). Primer sequences are available in Supplementary Table 1.

Statistics

Data are presented as mean ± S.E.M. N represents biological replicates and all experiments were replicated in at least two independent cell isolations. Changes in gene expression presented in Figure 3C were calculated using $\log_2$ transformed values where fold changes were calculated by taking the normalized ($mean_{stretch} - mean_{control}$) with a S.E.M being $\sqrt{((SD_{control}^2 / n_{control}) + (SD_{stretch}^2/n_{stretch}))}$. Statistical analysis was performed using GraphPad Prism 6. Normal distribution of data was determined by D'Agostino & Pearson omnibus normality test and assisted in the choice of subsequent parametric or non-parametric statistical tests. For comparison of two groups, two-sided Student's *t*-test or Mann-Whitney testing was used. If multiple t-tests were performed, these were corrected for multiple comparisons using the Holm-Sidak *post hoc* test. For comparison between three or more groups one-way ANOVA with Tukey's *post hoc* testing (parametric) and Kruskal-Wallis with Dunn's *post hoc* testing (non-parametric) was used. For data sets comparing two interventions (e.g. substrate stiffness and stretch), two-way ANOVA with the Tukey's *post hoc* test was used. For correlation of parametric data, Pearson's test was used. ***P<0.005, **P<0.01, *P<0.05.

Acknowledgements
The authors would like to thank Jennifer Stowe, Vandya Juneja, and Joey Ochoa for excellent technical assistance and Jeffrey H. Omens for valuable scientific input. The authors are grateful for the funding from The Research Council of Norway (K.M.H.), the European Commission program (K.M.H.), the NSF Graduate Research Fellowship Program (A.K.), grants R01CA206880 and DP2OD006460 (A.J.E). This work was supported in part by the National Institutes of Health *via* grants GM094503, GM103426, HL105242, HL122199 and HL105242, and California Institute of Regenerative Medicine grant CIRM RT3-07899. A.D.M is a co-founder, scientific advisor and equity-holder of Insilicomed, Inc., a licensee of UC San Diego software that was not used in this research. Insilicomed, Inc. had no involvement at all in design, performance, analysis or funding of the present study. This relationship has been disclosed to, reviewed, and approved by the University of California San Diego in accordance with its conflict of interest policies. The other authors have no relationships to disclose.

References

Antoniades, H.N., Scher, C.D., and Stiles, C.D. (1979). Purification of human platelet-derived growth factor. Proc Natl Acad Sci U S A *76*, 1809-1813.
Berry, M.F., Engler, A.J., Woo, Y.J., Pirolli, T.J., Bish, L.T., Jayasankar, V., Morine, K.J., Gardner, T.J., Discher, D.E., and Sweeney, H.L. (2006). Mesenchymal stem cell injection after myocardial infarction improves myocardial compliance. Am J Physiol Heart Circ Physiol *290*, H2196-2203.
Biernacka, A., Dobaczewski, M., and Frangogiannis, N.G. (2011). TGF-beta signaling in fibrosis. Growth Factors *29*, 196-202.
Caliari, S.R., Perepelyuk, M., Cosgrove, B.D., Tsai, S.J., Lee, G.Y., Mauck, R.L., Wells, R.G., and Burdick, J.A. (2016). Stiffening hydrogels for investigating the dynamics of hepatic stellate cell mechanotransduction during myofibroblast activation. Sci Rep *6*, 21387.
Camelliti, P., Gallagher, J.O., Kohl, P., and McCulloch, A.D. (2006). Micropatterned cell cultures on elastic membranes as an in vitro model of myocardium. Nat Protoc *1*, 1379-1391.
Carraher, C.L., and Schwarzbauer, J.E. (2013). Regulation of matrix assembly through rigidity-dependent fibronectin conformational changes. J Biol Chem *288*, 14805-14814.
Chitu, V., and Stanley, E.R. (2006). Colony-stimulating factor-1 in immunity and inflammation. Curr Opin Immunol *18*, 39-48.
Creemers, E.E., and Pinto, Y.M. (2011). Molecular mechanisms that control interstitial fibrosis in the pressure-overloaded heart. Cardiovasc Res *89*, 265-272.
Cui, Y., Hameed, F.M., Yang, B., Lee, K., Pan, C.Q., Park, S., and Sheetz, M. (2015). Cyclic stretching of soft substrates induces spreading and growth. Nat Commun *6*, 6333.
Daskalopoulos, E.P., Janssen, B.J., and Blankesteijn, W.M. (2012). Myofibroblasts in the infarct area: concepts and challenges. Microsc Microanal *18*, 35-49.
Davis, J., and Molkentin, J.D. (2014). Myofibroblasts: trust your heart and let fate decide. J Mol Cell Cardiol *70*, 9-18.

Duerr, G.D., Elhafi, N., Bostani, T., Ellinger, J., Swieny, L., Kolobara, E., Welz, A., and Dewald, O. (2011). Comparison of myocardial remodeling between cryoinfarction and reperfused infarction in mice. J Biomed Biotechnol *2011*, 961298.
Ehler, E., Moore-Morris, T., and Lange, S. (2013). Isolation and culture of neonatal mouse cardiomyocytes. J Vis Exp.
Engebretsen, K.V., Lunde, I.G., Strand, M.E., Waehre, A., Sjaastad, I., Marstein, H.S., Skrbic, B., Dahl, C.P., Askevold, E.T., Christensen, G., Bjornstad, J.L., and Tonnessen, T. (2013). Lumican is increased in experimental and clinical heart failure, and its production by cardiac fibroblasts is induced by mechanical and proinflammatory stimuli. FEBS J *280*, 2382-2398.
Engler, A.J., Carag-Krieger, C., Johnson, C.P., Raab, M., Tang, H.Y., Speicher, D.W., Sanger, J.W., Sanger, J.M., and Discher, D.E. (2008). Embryonic cardiomyocytes beat best on a matrix with heart-like elasticity: scar-like rigidity inhibits beating. J Cell Sci *121*, 3794-3802.
Goffin, J.M., Pittet, P., Csucs, G., Lussi, J.W., Meister, J.J., and Hinz, B. (2006). Focal adhesion size controls tension-dependent recruitment of alpha-smooth muscle actin to stress fibers. J Cell Biol *172*, 259-268.
Guo, Y., Zeng, Q.C., Zhang, C.Q., Zhang, X.Z., Li, R.X., Wu, J.M., Guan, J., Liu, L., Zhang, X.C., Li, J.Y., and Wan, Z.M. (2013). Extracellular matrix of mechanically stretched cardiac fibroblasts improves viability and metabolic activity of ventricular cells. Int J Med Sci *10*, 1837-1845.
Guvendiren, M., and Burdick, J.A. (2012). Stiffening hydrogels to probe short- and long-term cellular responses to dynamic mechanics. Nat Commun *3*, 792.
Guvendiren, M., Perepelyuk, M., Wells, R.G., and Burdick, J.A. (2014). Hydrogels with differential and patterned mechanics to study stiffness-mediated myofibroblastic differentiation of hepatic stellate cells. J Mech Behav Biomed Mater *38*, 198-208.
Gwechenberger, M., Mendoza, L.H., Youker, K.A., Frangogiannis, N.G., Smith, C.W., Michael, L.H., and Entman, M.L. (1999). Cardiac myocytes produce interleukin-6 in culture and in viable border zone of reperfused infarctions. Circulation *99*, 546-551.
Hermans, K.C., Daskalopoulos, E.P., and Blankesteijn, W.M. (2016). The Janus face of myofibroblasts in the remodeling heart. J Mol Cell Cardiol *91*, 35-41.
Herum, K.M., Lunde, I.G., Skrbic, B., Florholmen, G., Behmen, D., Sjaastad, I., Carlson, C.R., Gomez, M.F., and Christensen, G. (2013). Syndecan-4 signaling via NFAT regulates extracellular matrix production and cardiac myofibroblast differentiation in response to mechanical stress. J Mol Cell Cardiol *54*, 73-81.
Herum, K.M., Lunde, I.G., Skrbic, B., Louch, W.E., Hasic, A., Boye, S., Unger, A., Brorson, S.H., Sjaastad, I., Tonnessen, T., Linke, W.A., Gomez, M.F., and Christensen, G. (2015). Syndecan-4 is a key determinant of collagen cross-linking and passive myocardial stiffness in the pressure-overloaded heart. Cardiovasc Res *106*, 217-226.
Hinz, B. (2007). Formation and function of the myofibroblast during tissue repair. J Invest Dermatol *127*, 526-537.
Hohensinner, P.J., Kaun, C., Rychli, K., Niessner, A., Pfaffenberger, S., Rega, G., de Martin, R., Maurer, G., Ullrich, R., Huber, K., and Wojta, J. (2007). Macrophage colony stimulating factor expression in human cardiac cells is upregulated by tumor necrosis factor-alpha via an NF-kappaB dependent mechanism. J Thromb Haemost *5*, 2520-2528.
Husse, B., Briest, W., Homagk, L., Isenberg, G., and Gekle, M. (2007). Cyclical mechanical stretch modulates expression of collagen I and collagen III by PKC and tyrosine kinase in cardiac fibroblasts. Am J Physiol Regul Integr Comp Physiol *293*, R1898-1907.
Hynes, R.O. (2002). Integrins: bidirectional, allosteric signaling machines. Cell *110*, 673-687.
Imanaka-Yoshida, K., Hiroe, M., Nishikawa, T., Ishiyama, S., Shimojo, T., Ohta, Y., Sakakura, T., and Yoshida, T. (2001). Tenascin-C modulates adhesion of cardiomyocytes to extracellular matrix during tissue remodeling after myocardial infarction. Lab Invest *81*, 1015-1024.

Ingber, D.E. (2008). Tensegrity and mechanotransduction. J Bodyw Mov Ther *12*, 198-200.
Jiang, Z., Zhong, G., Wen, L., Hong, Y., Fang, S., Sun, P., Li, S., Li, S., and Feng, G. (2016). The Role of Platelet-Derived Growth Factor-B/Platelet-Derived Growth Factor Receptor-beta Signaling in Chronic Atrial Fibrillation. Cardiology *133*, 242-256.
Kasner, M., Westermann, D., Lopez, B., Gaub, R., Escher, F., Kuhl, U., Schultheiss, H.P., and Tschope, C. (2011). Diastolic tissue Doppler indexes correlate with the degree of collagen expression and cross-linking in heart failure and normal ejection fraction. J Am Coll Cardiol *57*, 977-985.
Kloxin, A.M., Benton, J.A., and Anseth, K.S. (2010). In situ elasticity modulation with dynamic substrates to direct cell phenotype. Biomaterials *31*, 1-8.
Lee, A.A., Delhaas, T., McCulloch, A.D., and Villarreal, F.J. (1999). Differential responses of adult cardiac fibroblasts to in vitro biaxial strain patterns. J Mol Cell Cardiol *31*, 1833-1843.
Li, C.X., Talele, N.P., Boo, S., Koehler, A., Knee-Walden, E., Balestrini, J.L., Speight, P., Kapus, A., and Hinz, B. (2017). MicroRNA-21 preserves the fibrotic mechanical memory of mesenchymal stem cells. Nat Mater *16*, 379-389.
Li, Z., Dranoff, J.A., Chan, E.P., Uemura, M., Sevigny, J., and Wells, R.G. (2007). Transforming growth factor-beta and substrate stiffness regulate portal fibroblast activation in culture. Hepatology *46*, 1246-1256.
Lighthouse, J.K., and Small, E.M. (2016). Transcriptional control of cardiac fibroblast plasticity. J Mol Cell Cardiol *91*, 52-60.
Lindsey, M.L., Zouein, F.A., Tian, Y., Padmanabhan Iyer, R., and de Castro Bras, L.E. (2015). Osteopontin is proteolytically processed by matrix metalloproteinase 9. Can J Physiol Pharmacol *93*, 879-886.
Liu, F., Lagares, D., Choi, K.M., Stopfer, L., Marinkovic, A., Vrbanac, V., Probst, C.K., Hiemer, S.E., Sisson, T.H., Horowitz, J.C., Rosas, I.O., Fredenburgh, L.E., Feghali-Bostwick, C., Varelas, X., Tager, A.M., and Tschumperlin, D.J. (2015). Mechanosignaling through YAP and TAZ drives fibroblast activation and fibrosis. Am J Physiol Lung Cell Mol Physiol *308*, L344-357.
Lopez, B., Gonzalez, A., Lindner, D., Westermann, D., Ravassa, S., Beaumont, J., Gallego, I., Zudaire, A., Brugnolaro, C., Querejeta, R., Larman, M., Tschope, C., and Diez, J. (2013). Osteopontin-mediated myocardial fibrosis in heart failure: a role for lysyl oxidase? Cardiovasc Res *99*, 111-120.
Lopez, B., Querejeta, R., Gonzalez, A., Larman, M., and Diez, J. (2012). Collagen cross-linking but not collagen amount associates with elevated filling pressures in hypertensive patients with stage C heart failure: potential role of lysyl oxidase. Hypertension *60*, 677-683.
Lunde, I.G., Herum, K.M., Carlson, C.C., and Christensen, G. (2016). Syndecans in heart fibrosis. Cell Tissue Res *365*, 539-552.
Luther, D.J., Thodeti, C.K., Shamhart, P.E., Adapala, R.K., Hodnichak, C., Weihrauch, D., Bonaldo, P., Chilian, W.M., and Meszaros, J.G. (2012). Absence of type VI collagen paradoxically improves cardiac function, structure, and remodeling after myocardial infarction. Circ Res *110*, 851-856.
Maruhashi, T., Kii, I., Saito, M., and Kudo, A. (2010). Interaction between periostin and BMP-1 promotes proteolytic activation of lysyl oxidase. J Biol Chem *285*, 13294-13303.
Mazhari, R., Omens, J.H., Covell, J.W., and McCulloch, A.D. (2000). Structural basis of regional dysfunction in acutely ischemic myocardium. Cardiovasc Res *47*, 284-293.
McCulloch, A.D. (2016). Systems Biophysics: Multiscale Biophysical Modeling of Organ Systems. Biophys J *110*, 1023-1027.
Melchior-Becker, A., Dai, G., Ding, Z., Schafer, L., Schrader, J., Young, M.F., and Fischer, J.W. (2011). Deficiency of biglycan causes cardiac fibroblasts to differentiate into a myofibroblast phenotype. J Biol Chem *286*, 17365-17375.
Melleby, A.O., Strand, M.E., Romaine, A., Herum, K.M., Skrbic, B., Dahl, C.P., Sjaastad, I., Fiane, A.E., Filmus, J., Christensen, G., and Lunde, I.G. (2016). The Heparan Sulfate Proteoglycan Glypican-6 Is

Upregulated in the Failing Heart, and Regulates Cardiomyocyte Growth through ERK1/2 Signaling. PLoS One *11*, e0165079.
Molkentin, J.D., Bugg, D., Ghearing, N., Dorn, L.E., Kim, P., Sargent, M.A., Gunaje, J., Otsu, K., and Davis, J.M. (2017). Fibroblast-Specific Genetic Manipulation of p38 MAPK in vivo Reveals its Central Regulatory Role in Fibrosis. Circulation.
Mukherjee, D., and Sen, S. (1990). Collagen phenotypes during development and regression of myocardial hypertrophy in spontaneously hypertensive rats. Circ Res *67*, 1474-1480.
Nakazawa, N., Sathe, A.R., Shivashankar, G.V., and Sheetz, M.P. (2016). Matrix mechanics controls FHL2 movement to the nucleus to activate p21 expression. Proc Natl Acad Sci U S A *113*, E6813-E6822.
Olsen, A.L., Bloomer, S.A., Chan, E.P., Gaca, M.D., Georges, P.C., Sackey, B., Uemura, M., Janmey, P.A., and Wells, R.G. (2011). Hepatic stellate cells require a stiff environment for myofibroblastic differentiation. Am J Physiol Gastrointest Liver Physiol *301*, G110-118.
Ondeck, M.G., and Engler, A.J. (2016). Mechanical Characterization of a Dynamic and Tunable Methacrylated Hyaluronic Acid Hydrogel. J Biomech Eng *138*, 021003.
Papakrivopoulou, J., Lindahl, G.E., Bishop, J.E., and Laurent, G.J. (2004). Differential roles of extracellular signal-regulated kinase 1/2 and p38MAPK in mechanical load-induced procollagen alpha1(I) gene expression in cardiac fibroblasts. Cardiovasc Res *61*, 736-744.
Parsons, J.T. (2003). Focal adhesion kinase: the first ten years. J Cell Sci *116*, 1409-1416.
Rasi, K., Piuhola, J., Czabanka, M., Sormunen, R., Ilves, M., Leskinen, H., Rysa, J., Kerkela, R., Janmey, P., Heljasvaara, R., Peuhkurinen, K., Vuolteenaho, O., Ruskoaho, H., Vajkoczy, P., Pihlajaniemi, T., and Eklund, L. (2010). Collagen XV is necessary for modeling of the extracellular matrix and its deficiency predisposes to cardiomyopathy. Circ Res *107*, 1241-1252.
Schellings, M.W., Vanhoutte, D., Swinnen, M., Cleutjens, J.P., Debets, J., van Leeuwen, R.E., d'Hooge, J., Van de Werf, F., Carmeliet, P., Pinto, Y.M., Sage, E.H., and Heymans, S. (2009). Absence of SPARC results in increased cardiac rupture and dysfunction after acute myocardial infarction. J Exp Med *206*, 113-123.
Simmons, C.S., Ribeiro, A.J., and Pruitt, B.L. (2013). Formation of composite polyacrylamide and silicone substrates for independent control of stiffness and strain. Lab Chip *13*, 646-649.
Skrbic, B., Engebretsen, K.V., Strand, M.E., Lunde, I.G., Herum, K.M., Marstein, H.S., Sjaastad, I., Lunde, P.K., Carlson, C.R., Christensen, G., Bjornstad, J.L., and Tonnessen, T. (2015). Lack of collagen VIII reduces fibrosis and promotes early mortality and cardiac dilatation in pressure overload in mice. Cardiovasc Res *106*, 32-42.
Spinale, F.G., Frangogiannis, N.G., Hinz, B., Holmes, J.W., Kassiri, Z., and Lindsey, M.L. (2016). Crossing Into the Next Frontier of Cardiac Extracellular Matrix Research. Circ Res *119*, 1040-1045.
Sullivan, K.E., Quinn, K.P., Tang, K.M., Georgakoudi, I., and Black, L.D., 3rd. (2014). Extracellular matrix remodeling following myocardial infarction influences the therapeutic potential of mesenchymal stem cells. Stem Cell Res Ther *5*, 14.
Takahashi, S., Barry, A.C., and Factor, S.M. (1990). Collagen degradation in ischaemic rat hearts. Biochem J *265*, 233-241.
Tarzami, S.T., Cheng, R., Miao, W., Kitsis, R.N., and Berman, J.W. (2002). Chemokine expression in myocardial ischemia: MIP-2 dependent MCP-1 expression protects cardiomyocytes from cell death. J Mol Cell Cardiol *34*, 209-221.
Tomasek, J.J., Gabbiani, G., Hinz, B., Chaponnier, C., and Brown, R.A. (2002). Myofibroblasts and mechano-regulation of connective tissue remodelling. Nat Rev Mol Cell Biol *3*, 349-363.
Tse, J.R., and Engler, A.J. (2010). Preparation of hydrogel substrates with tunable mechanical properties. Curr Protoc Cell Biol *Chapter 10*, Unit 10 16.
van Putten, S., Shafieyan, Y., and Hinz, B. (2016). Mechanical control of cardiac myofibroblasts. J Mol Cell Cardiol *93*, 133-142.

Virag, J.I., and Murry, C.E. (2003). Myofibroblast and endothelial cell proliferation during murine myocardial infarct repair. Am J Pathol *163*, 2433-2440.
Wang, J., Chen, H., Seth, A., and McCulloch, C.A. (2003). Mechanical force regulation of myofibroblast differentiation in cardiac fibroblasts. Am J Physiol Heart Circ Physiol *285*, H1871-1881.
Waxman, A.S., Kornreich, B.G., Gould, R.A., Moise, N.S., and Butcher, J.T. (2012). Interactions between TGFbeta1 and cyclic strain in modulation of myofibroblastic differentiation of canine mitral valve interstitial cells in 3D culture. J Vet Cardiol *14*, 211-221.
Willems, I.E., Arends, J.W., and Daemen, M.J. (1996). Tenascin and fibronectin expression in healing human myocardial scars. J Pathol *179*, 321-325.
Wong, V.W., Longaker, M.T., and Gurtner, G.C. (2012). Soft tissue mechanotransduction in wound healing and fibrosis. Semin Cell Dev Biol *23*, 981-986.
Yeung, T., Georges, P.C., Flanagan, L.A., Marg, B., Ortiz, M., Funaki, M., Zahir, N., Ming, W., Weaver, V., and Janmey, P.A. (2005). Effects of substrate stiffness on cell morphology, cytoskeletal structure, and adhesion. Cell Motil Cytoskeleton *60*, 24-34.
Zeigler, A.C., Richardson, W.J., Holmes, J.W., and Saucerman, J.J. (2016). A computational model of cardiac fibroblast signaling predicts context-dependent drivers of myofibroblast differentiation. J Mol Cell Cardiol *94*, 72-81.
Zhang, J., Fan, G., Zhao, H., Wang, Z., Li, F., Zhang, P., Zhang, J., Wang, X., and Wang, W. (2017). Targeted inhibition of Focal Adhesion Kinase Attenuates Cardiac Fibrosis and Preserves Heart Function in Adverse Cardiac Remodeling. Sci Rep *7*, 43146.
Zhao, W., Zhao, T., Huang, V., Chen, Y., Ahokas, R.A., and Sun, Y. (2011). Platelet-derived growth factor involvement in myocardial remodeling following infarction. J Mol Cell Cardiol *51*, 830-838.

Figure Legends

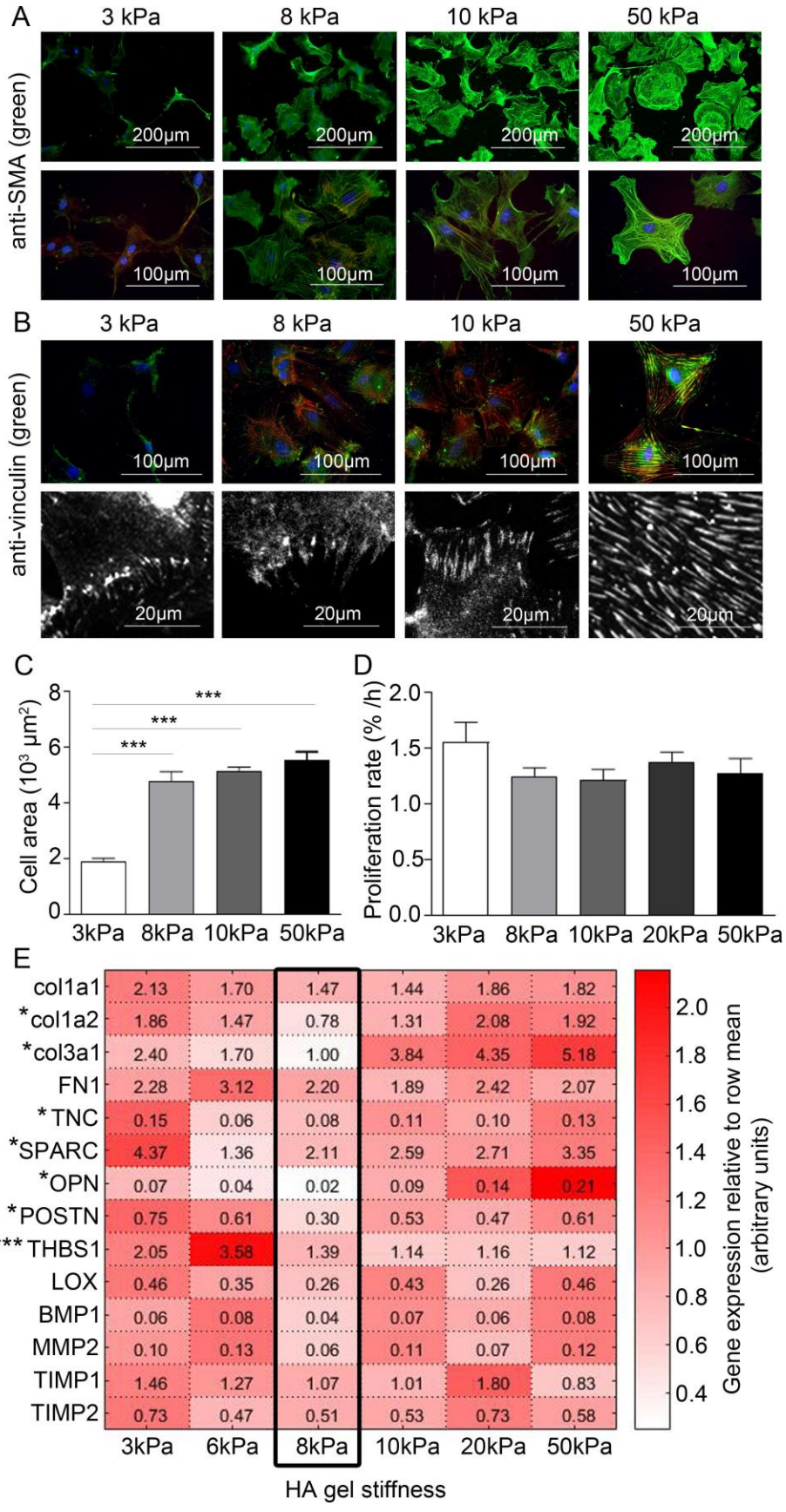
A
3 kPa
8 kPa
10 kPa
50 kPa
anti-SMA (green)
200µm
100µm
B
anti-vinculin (green)
100µm
20µm
C
Cell area (10³ µm²)
***
3kPa 8kPa 10kPa 50kPa
D
Proliferation rate (% /h)
3kPa 8kPa 10kPa 20kPa 50kPa
E
col1a1 2.13 1.70 1.47 1.44 1.86 1.82
*col1a2 1.86 1.47 0.78 1.31 2.08 1.92
*col3a1 2.40 1.70 1.00 3.84 4.35 5.18
FN1 2.28 3.12 2.20 1.89 2.42 2.07
*TNC 0.15 0.06 0.08 0.11 0.10 0.13
*SPARC 4.37 1.36 2.11 2.59 2.71 3.35
*OPN 0.07 0.04 0.02 0.09 0.14 0.21
*POSTN 0.75 0.61 0.30 0.53 0.47 0.61
***THBS1 2.05 3.58 1.39 1.14 1.16 1.12
LOX 0.46 0.35 0.26 0.43 0.26 0.46
BMP1 0.06 0.08 0.04 0.07 0.06 0.08
MMP2 0.10 0.13 0.06 0.11 0.07 0.12
TIMP1 1.46 1.27 1.07 1.01 1.80 0.83
TIMP2 0.73 0.47 0.51 0.53 0.73 0.58
3kPa 6kPa 8kPa 10kPa 20kPa 50kPa
HA gel stiffness
Gene expression relative to row mean (arbitrary units)

Figure 1. Maintaining a quiescent cardiac fibroblast phenotype by controlling substrate stiffness. Immunofluorescent staining for smooth muscle α-actin (SMA; green) in (A) and vinculin in (B). F-actin and nuclei were stained with phalloidin (red) and DAPI (blue), respectively. (C) Cell area and (D) proliferation rate (% of proliferating cells per hour) of cardiac fibroblasts plated on gels of 3, 8, 10, 20 and 50kPa hyaluronic acid (HA) gels. One-way ANOVA with Tukey's post hoc test was used in C and D. N=6 and 4, respectively. (E) Heatmap showing relative mRNA expression levels of collagen (col) 1a1, 1a2 and 3a1, fibronectin (FN1), tenascin C (TNC), secreted protein acidic and rich in cysteine (SPARC), osteopontin (OPN), periostin (POSTN), thrombospondin 1 (THBS1), lysyl oxidase (LOX), bone morphogenetic protein 1 (BMP1), matrix metalloproteinase (MMP) 2, tissue inhibitor of metalloproteinase (TIMP) 1 and TIMP2 normalized to glyceraldehyde 3-phosphate dehydrogenase (GAPDH) in cardiac fibroblasts plated on HA gels with 3, 6, 8, 10, 20 and 50kPa stiffness. Expression across genes was lowest at 8kPa stiffness as indicated by the black frame. Values in each box represent raw 2^(-delta Ct) values for comparison of expression levels among genes. *Denotes significant effect of stiffness as tested by one-way ANOVA and Kruskal-Wallis tests for parametric and non-parametric data, respectively. N=8-12

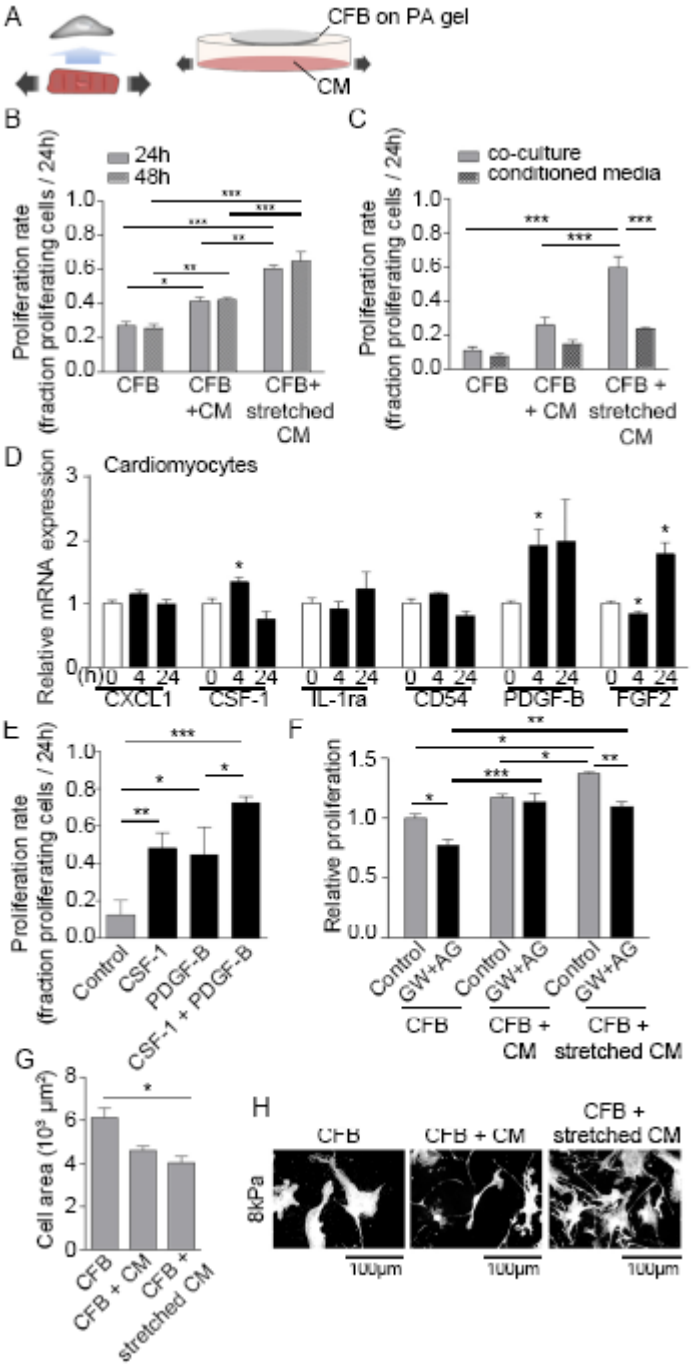

Figure 2. Paracrine signaling from stretched cardiomyocytes induces cardiac fibroblast proliferation. (A) Schematic illustration of the principles of the paracrine signaling model. (B) Proliferation rate of cardiac fibroblast (CFB) cultures alone, or in co-culture with non-stretched cardiomyocytes (CM) or stretched CM. CFB were plated on PA gels with 8kPa stiffness. Two-way ANOVA showed significant effect of culture type*** and Tukey's post hoc test as indicated in figures. N=3-6. (C) Proliferation rate of CFB in CM co-culture or treated with conditioned media from co-cultures. Two-way ANOVA showed an effect of cuture type***, conditioned media*** and a significant interaction**. Tukey's post hoc test results are indicated in figures.

N=3. (D) Relative expression of chemokine (C-X-C motif) ligand 1 (CXCL1), colony stimulating factor 1 (CSF-1), interleukin-1 receptor antagonist (IL-1ra), cluster of differentiation 54 (CD54), platelet-derived growth factor B (PDGF-B) and fibroblast growth factor 2 (FGF2) mRNA normalized to glyceraldehyde 3-phosphate dehydrogenase (GAPDH) mRNA in CM stretched for 4 and 24h. *Denotes significant difference from 0h control as determined by Student's t-test. N=9 (control) and 4 (stretch). (E) Proliferation rate following 24h stimulation with recombinant CSF-1 and/or PDGF-B. One-way ANOVA showed significant effect of stimulation*** and Tukey's post hoc test results as indicated. N=3. (F) Relative proliferation rate of CFB in co-cultures in the presence of PDGF-B and CSF-1 receptor antagonists (AG and GW, respectively). Two-way ANOVA showed an effect of culture type*** and blockers*** as well as significant interaction* between the two. Tukey's post hoc test results are indicated in figure. N=3. Cell area (G) and morphology (H) of CFB on 8kPa alone, or in co-culture with non-stretched and stretched CM. One-way ANOVA showed significant effect of culture type* on cell area and Tukey's post hoc test results as indicated in figure.

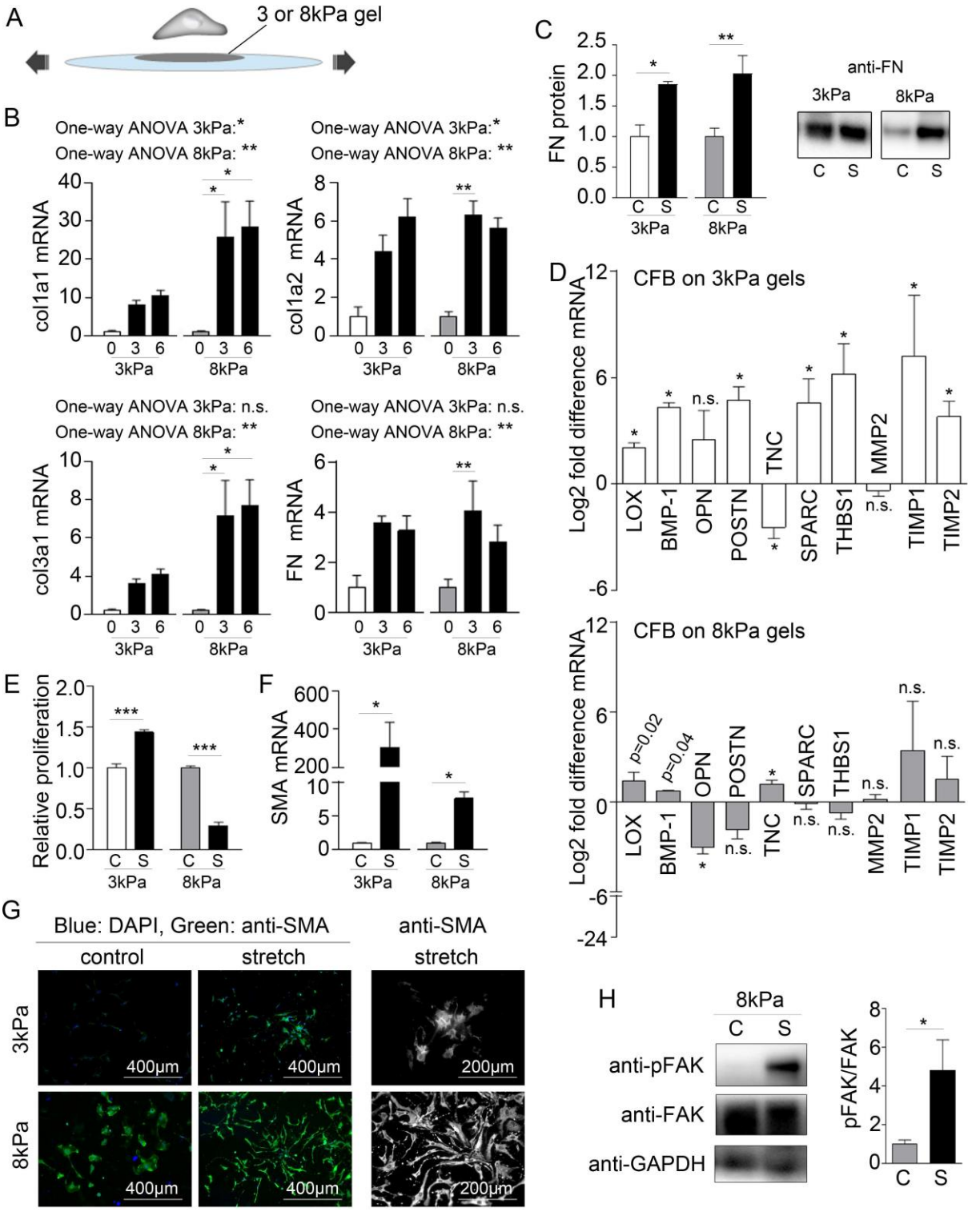

Figure 3. Stretch promotes extracellular matrix remodeling by CFB. (A) Schematic illustration of the principles of the stretch model. (B) Collagen (col) 1a1, 1a2 and 3a1 and fibronectin (FN1) mRNA normalized to glyceraldehyde 3-phosphate dehydrogenase (GAPDH) mRNA in cardiac fibroblasts on 3 and 8kPa gels subjected to 0, 3 and 6% stretch (x-axis). One-way ANOVA was used to test significant effect of stretch with Tukey's post hoc tests for specific comparisons.

Statistical results are indicated in the figure. N=4 (control) and 12 (stretch). (C) Quantification and immunoblot of fibronectin (FN) protein normalized to total protein determined by Ponceau staining. N=4 (3kPa) and 8 for (8kPa). (D) Fold difference in lysyl oxidase (LOX), bone morphogenetic protein 1 (BMP-1), osteopontin (OPN), periostin (POSTN), tenascin C (TNC), secreted protein acidic and rich in cysteine (SPARC), thrombospondin 1 (THBS1), metalloproteinase (MMP) 2, and tissue inhibitor of metalloproteinase (TIMP) 1 and 2 mRNA expression normalized to GAPDH mRNA. Significance was determined by multiple Student's t-tests corrected for multiple comparisons using Holm-Sidak's post hoc test. P-values displayed in figure D are the uncorrected p-values from the t-test. N=4 (control) and 12 (stretch). (E) Relative proliferation of CFB controls (C) or with 3% stretch (S). N=3. (F) Smooth muscle a-actin (SMA) mRNA normalized to GAPDH mRNA. N=4 (control) and 12 (stretch). (G) Immunofluorescent staining for SMA (green) and DAPI staining for nuclei (blue). (H) Immunoblot for total and phophorylated focal adhesion kinase (FAK and pFAK, respectively) normalized to GAPDH. N=4. Student's t-test was used to determine significant changes for C, E, F and H.

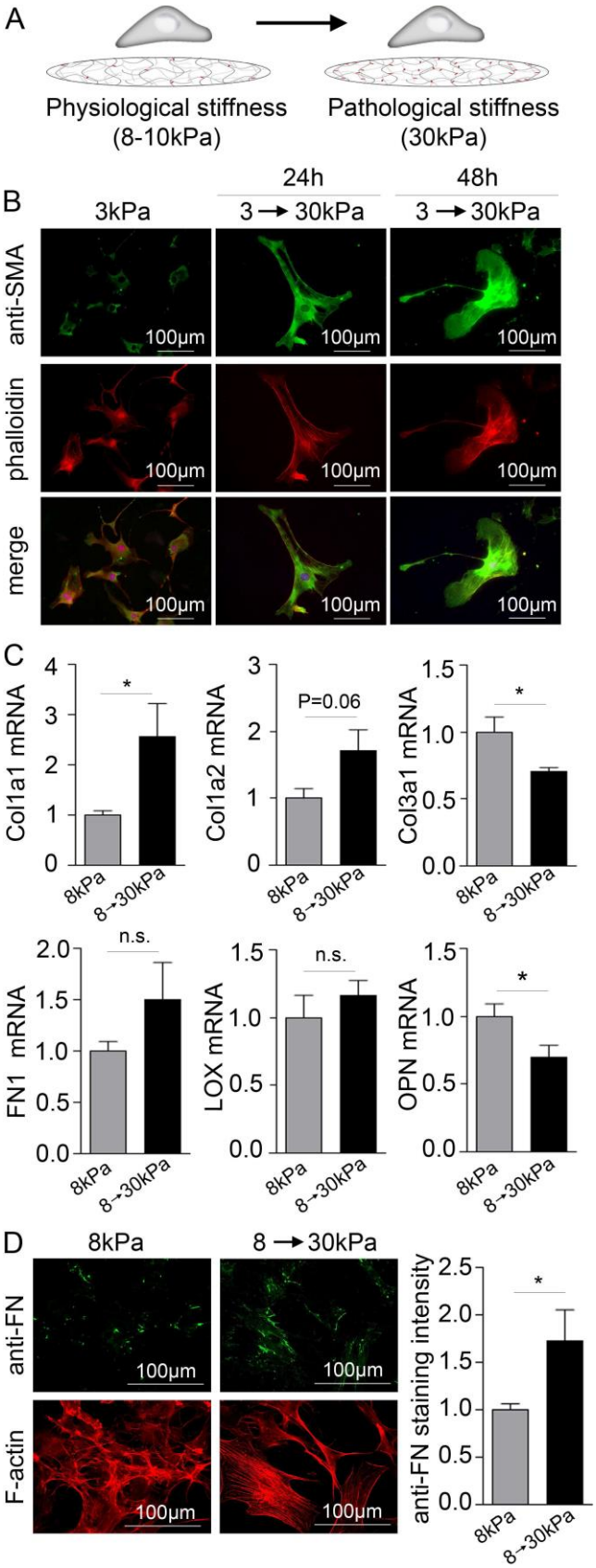
A
Physiological stiffness
(8-10kPa)
Pathological stiffness
(30kPa)
B
24h
48h
3kPa
3 → 30kPa
3 → 30kPa
anti-SMA
phalloidin
merge
100μm
C
Col1a1 mRNA
Col1a2 mRNA
Col3a1 mRNA
FN1 mRNA
LOX mRNA
OPN mRNA
P=0.06
n.s.
8kPa
8→30kPa
D
8kPa
8 → 30kPa
anti-FN
F-actin
anti-FN staining intensity

Figure 4. Matrix stiffening causes cell spreading, smooth muscle a-actin fiber formation, upregulation of collagen I and downregulation of collagen III. (A) Schematic illustration of the principles of the stiffening model. (B) Immunofluorescent staining for smooth muscle a-actin (SMA; green). F-actin and nuclei were stained with phalloidin (red) and DAPI (blue), respectively. (C) Collagen (col) 1a1, 1a2 and 3a1, fibronectin (FN1), lysyl oxidase (LOX) and osteopontin (OPN) mRNA normalized to glyceraldehyde 3-phosphate dehydrogenase (GAPDH) mRNA in cardiac fibroblasts on 8kPa gels stiffened to 30kPa. N=4 (control) and 12 (stiffened). (D) Immunofluorescent staining for fibronectin (FN; green) and quantification of staining intensity 48h after gels stiffening. N=8. F-actin was stained with phalloidin (red). Student's t-tests were applied to determine significant changes.

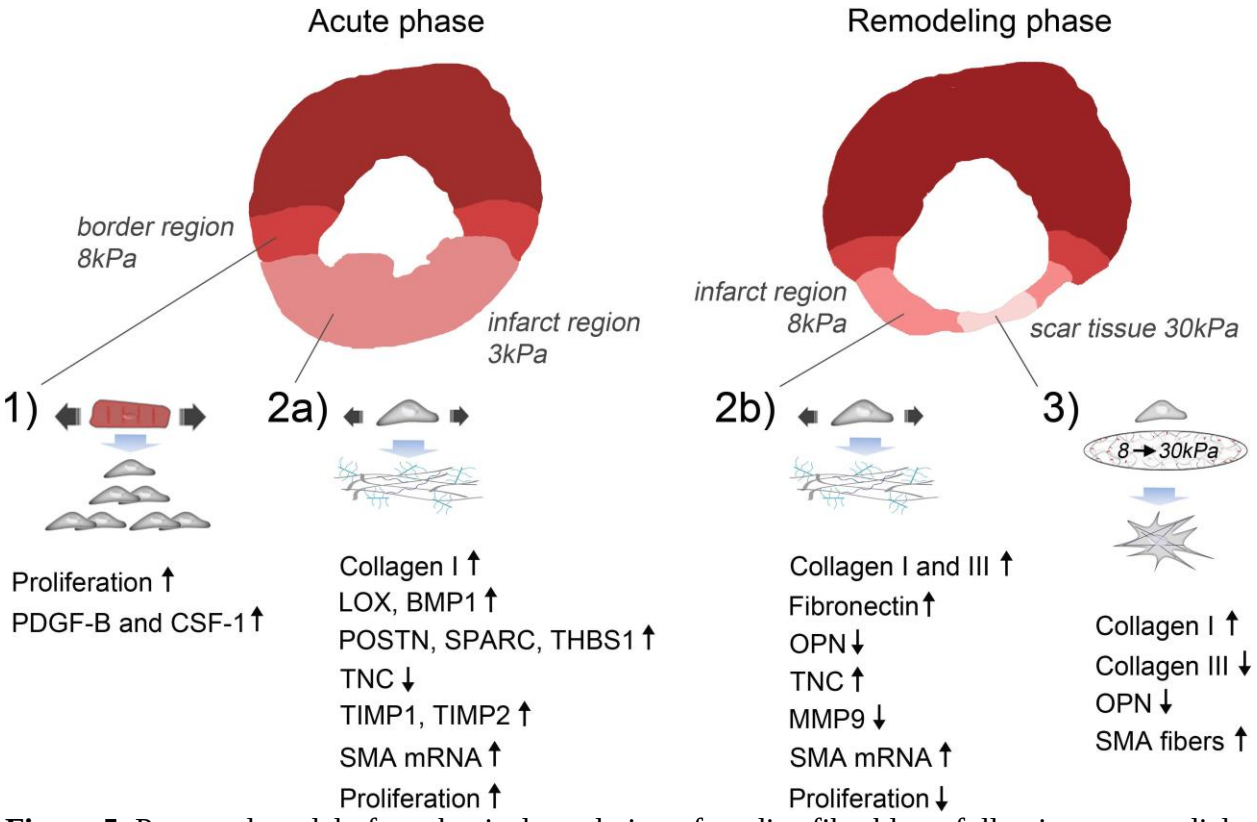

Figure 5. Proposed model of mechanical regulation of cardiac fibroblasts following myocardial infarction. 1) Paracrine signaling involving platelet-derived growth factor B (PDGF-B) and colony stimulating factor 1 (CSF-1) from stretched cardiomyocytes in the border region leads to proliferation of cardiac fibroblasts (CFB). 2a) Stretch of the infarct region during the acute phase after myocardial infarction (extracellular matrix (ECM) stiffness ~ 3kPa) promotes collagen I, lysyl oxidase (LOX), bone morphogenetic protein 1 (BMP-1), periostin (POSTN), secreted protein acidic and rich in cysteine (SPARC), thrombospondin 1 (THBS1), tissue inhibitor of metalloproteinase (TIMP) 1 and 2 while inhibits tenascin C (TNC) expression by CFB. Proliferation is increased during this phase; 2b) Stretch of the infarct region during the remodeling phase (ECM stiffness ~ 8kPa) also upregulates collagen I in addition to collagen III, fibronectin and TNC, while downregulates the matricellular protein osteopontin (OPN). Matrix metalloproteinase 9 (MMP9) expression was reduced in this setting. Proliferation is decreased during this phase. Stretch causes upregulation of smooth muscle a-actin (SMA) mRNA during both the acute and remodeling phases; however incorporation into stress fibers requires an accompanying increase in matrix stiffness; 3) At late stages of infarct healing, ECM stiffening to pathological stiffnesses (~ 30kPa) dominates the mechanical environment. This promotes a contractile CFB phenotype due to SMA fiber formation that has elevated, albeit dampened collagen I production compared to that of stretched CFB. Collagen III and osteopontin (OPN) expression is reduced supporting scar maturation and healing. However, continuous stretch of CFB at this stage will cause persistent ECM production and thus development of pathological fibrosis.